Proceedings of the
44th IEEE Conference on Decision and Control, and
the European Control Conference 2005
Seville, Spain, December 12-15, 2005

Digital control of Fabry-Pérot interferometers

Enrico S. Canuto, *Member, IEEE*, Fabio Musso and Luca Massotti

***Abstract*—Fabry-Pérot interferometry (FPI) originally invented for spectroscopy is now evolving as a basic technology for ultra-fine dimensional stabilization and measurement. To this end, the light path length of an optical cavity and the wavelength of a laser source injected into the cavity have to be each other tuned through a set of frequency and/or displacement actuators driven by a sharp and narrow signal encoding total cavity detuning. Digital control is essential in facilitating and automating the FPI use in view of space applications and routine instrumentation. Embedded model control (EMC) developed by one of the authors has been employed. Experimental results are presented.**

I. Introduction

Fabry-Pèrot interferometer (FPI) was invented by the French physicists Fabry and Pérot at the end of the XIX century (1899) to enable high resolution observation of spectral lines. Multiple light reflection between two plane surfaces create interference patterns which being very sensible to wavelength and optical path length were employed in the course of the XX century as scanning spectrometers. A significant improvement was made since 1970 by piezo-tuning the FPI optical length and in 1984 the 1st application to the measurement of small displacements took place.

FPI made by vacuum cavities between two highly reflecting mirrors are employed for detecting gravitational waves in LIGO [10] and VIRGO [9] ground experiments and have been suggested as metrology lines for measuring and stabilizing linear/angular dimensions of space telescopes like GAIA [4]. One of the authors, working on this technology since 1998, implemented several digital control loops and automation to improve and facilitate FPI [3], [4], [5], [6].

PFI control problems and theirs solution to be mechanized into a Digital Control Unit (DCU) will be the subject of this paper. Section II will provide a brief illustration of FPI principles, applications and output signals to be fed back. Section III will present a unified treatment of the FPI control problems assuming multiple actuation [5] and Embedded Model Control (EMC) methodology [12], [13]. Section IV will present experimental results. Formulation will be free of theorem and proofs for sake of brevity.

This work was in part supported by grants from Alenia Spazio, Torino, Italy, within research projects sponsored by European Space Agency.

E. S. Canuto is with Politecnico di Torino, Dipartimento di Automatica e Informatica, Corso Duca degli Abruzzi 24, 10129, Torino, Italy (corresponding author: +39 011 5647026; fax: +39 011 5647099; e-mail: enrico.canuto@polito.it).

F. Musso, student, and L. Massotti are with Politecnico di Torino, Dipartimento di Automatica e Informatica, Italy (e-mail: fabio.musso@polito.it, luca.massotti@polito.it).

II. Fabry-Pérot interferometry

A. Basic principles and applications

Fabry-Pérot interferometers (FPI) treated in this paper are optical cavities [1] made by two aligned and highly reflecting mirrors where a laser light-wave is injected and a standing reflecting wave is created and kept either by regulating the incident wave frequency and/or by fine moving either mirror. As a result the cavity becomes an optical resonator as the injected light intensity is amplified inside the cavity. Intensity amplification is measured by the *cavity finesse* $\mathfrak{F}$ [1] which can reach values greater than 10^4. Any frequency perturbation of the incident light-wave as well as any perturbation of the optical path tends to destroy the standing reflecting wave condition by varying the intensity of the light-wave emitted by the cavity itself, which wave may be arranged to encode perturbation amplitude and sign.

Let $f_l = c/\lambda_l$ be the incident light frequency, typically 200 to 600 THz (from infrared to green), related to wavelength λ_l by the speed of light in vacuum c. Then denote cavity length with L, typically 0.01 to 100 m, measured along the optical axis joining the spot centres of the laser beam on each mirror. The standing wave condition implies an integer ratio between length and wavelength

$$L = N\lambda_l/2 \Rightarrow f_l L = Nc/2,\ N \text{ integer}. \qquad (1)$$

A pair (f_l, L) satisfying the above resonant condition is called a *resonant pair* and will be denoted as $(f_o(N), L_0(N))$. From (1), it is immediate that two successive resonant pairs indexed N, $N\pm1$ are separated in length by half-wavelength $\lambda_0/2$ and in frequency by the so-called *Free Spectral Range* (FSR)

$$F_0 = 0.5c/L_0 = 1/\tau_0, \qquad (2)$$

where τ_0 is the light travel time from mirror to mirror inside the cavity and $F_0 \simeq 150$ MHz @ $L_0 = 1$ m.

Actually, condition (1) can not be exactly met, but only approached, by forcing frequency and length to fluctuate around a resonant pair through active control. Thus by denoting length and frequency fluctuations (often called detuning) with $\Delta L = L - L_0(N)$ and $\Delta f = f_l - f_0(N)$ and fractional detuning with η, and by rewriting (1) as

$$\left(f_0 + \Delta f\right)\left(L_0 + \Delta L\right) = f_0 L_0 \left(1 + \eta\right) \tag{3}$$

a linear differential equation relating length and frequency detuning less the cavity detuning e can be written

$$\Delta f + \left(f_0 / L_0\right)\Delta L = e,\ e = f_0 \eta\,. \tag{4}$$

The above relation, called *lock-in condition*, holds only under sufficiently small detuning e, where small is dictated by cavity finesse $\mathfrak{F}$.

As the length-to-frequency scale $k_0 = f_0 / L_0$ is usually much greater than 10^{12} and frequency detuning Δf can be accurately measured below 1 Hz, FPI may reveal sub-atomic length detuning. This is achieved by revealing e through a suitable opto-electronics named after Pound and Drever (PD) [2] and by keeping e as small as possible through a control loop.

Accordingly, three main applications can be conceived:

1) *Length stabilization*: Δf is kept negligible by a frequency-stabilized laser source, which implies (4) to reduce to $\Delta L = L_0 e / f_0$ and to keep ΔL to zero by piezo-electric actuators (f.i. PZT ceramics) [3], [4].
2) *Frequency stabilization:* ΔL is kept negligible, for instance, by thermal control and ultra-low CTE (coefficient of thermal expansion) glass [7], which implies (4) to reduce to $\Delta f = e$. Then Δf is kept to zero by locking the incident laser frequency to cavity length by means of suitable frequency actuators (again PZT ceramics, thermal control, …) [5].
3) *Length measurement and tracking:* a frequency stabilized laser wave is detuned by a frequency actuator prior to be injected in the cavity so as to zero e in presence of a length detuning ΔL. The actuated Δf is made proportional to ΔL up to residual detuning e, laser instability and actuator noise. The scale factor f_0 / L_0 needs only to be calibrated for what concerns L_0 as f_0 is ensured by laser frequency stabilization. L_0 can be accurately measured by forcing frequency actuator to jump from current resonant condition N to $N \pm 1$. As ΔL may result from artificial and natural causes, f.i. thrust as in [6], FPI can be made to reveal microscopic phenomena.

In all applications, cavity detuning e plays the role of the performance variable to be kept close to zero.

B. *Response of PD chain and FPI performance*

The cavity detuning e is encoded in the emitted light-wave as the amplitude and phase of a radio-frequency modulation (typically $f_m \le 0.1 F_0$) applied to the incident laser beam and then revealed by demodulating the emitted light intensity collected by a photodiode. To dispose of a sharp zero-crossing at resonant condition (1), the demodulated amplitude V of $\sin\left(2\pi f_m\right)$ is employed as FPI measurement. The corresponding static response $V = h(e)$, frequency-to-voltage, is highly nonlinear (Fig. 1) and periodic (period equal to FSR F_0).

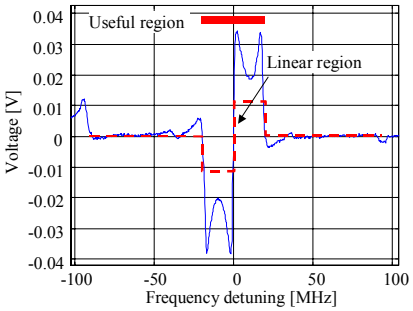

Fig. 1. Typical response of PD chain versus frequency detuning.

For control purposes, the normalized response, frequency-to-frequency, is defined

$$H(e) = h(e) / k_{\max},\ k_{\max} = 2V_{\max} / e_{\max}\,, \tag{5}$$

$V_{\max}$ being the peak voltage after zero crossing (resonant condition) and $e_{\max} \simeq 0.5 F_0 / \mathfrak{F}$ the corresponding frequency detuning. Only in the *useful region*, centered on zero crossing and large $2f_m$, $H(e)$ is different from zero and is a sector nonlinearity $[0,1]$. In a smaller region, the *linear region* large $2e_{\max}$, it becomes monotonic, undergoes a sharp zero crossing suitable for regulation/tracking and holds

$$H(e) = k_{\max} e / \left(1 + \left(e / e_{\max}\right)^2\right),\ \left|e / e_{\max}\right| \le 1\,. \tag{6}$$

In this sub-region the sector nonlinearity is $[0.5,1]$.

The values of the application [6], namely $L_0 = 0.195$ m and $\mathfrak{F} \cong 110$, yield $e_{\max} \cong 3.5$ MHz, which for a laser frequency $f_l = 563$ THz (green light) corresponds to an upper bound $e_{L,\max} \simeq 1.2$ nm in length units where to keep confined control residuals.

Neglecting PD dynamics, the measurement y_f in frequency units is related to e through the measurement error v and the response $H(e)$ as follows

$$y_f(t) = H(e) + v(t)\,. \tag{7}$$

By solving (7) for $e_L = e / k_0$, in length units, inside the linear region, and making cavity finesse $\mathfrak{F}$ explicit yields

$$e_L(t) \simeq \lambda_0 \left(y_f(t) - v(t)\right) / \left(4\mathfrak{F} e_{\max}\right),\ \lambda_0 = c / f_0 \tag{8}$$

FPI performance depends on (8), namely:

1) $y_f(t)/e_{\max}$, the fractional control jitter, depends on the closed-loop control bandwidth and on the residual noise, usually due to mechanical vibrations.
2) $v(t)/e_{\max}$, the fractional PD measurement error, depends on PD opto-electronics quality.
3) λ_0 varying from visible to infrared is about 1 μm.
4) *Ceteris paribus,* e is attenuated by increasing $\mathfrak{F}$.

As an example, the space astrometry mission GAIA [4] asks for an average length detuning less than 1 pm (RMS) over a length $L_0 \simeq 1$ m, where the average must be taken over $\tau = 3$ s. Then by assuming infrared wavelength $\lambda_0 \simeq 1.3$ μm and low finesse $\mathfrak{F} \simeq 150$, the target performance requires the average fractional jitter and PD noise to be less than 0.1%, a standard target.

III. Unified Digital Control Formulation

A. FPI control tasks

With reference to (5) and (6), two tasks are needed:

1) *Lock-in detection and recovery (LDR)* detects the presence of e outside the useful range due to onset and shocks and returns it to linear range (Fig. 2),
2) The *linear controller* operates under quasi-linear conditions, which are established as soon as e enters the linear range, i.e. $|e(t)| \le \bar{\eta} e_{\max}$, $\bar{\eta} < 1$.

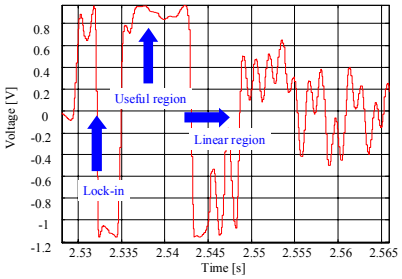

Fig. 2. Arduous LDR of a suspended cavity ([6]) under severe length detuning due to pendulum beat ($> 3e_{\max}$/ms).

Actually, the linear controller may operate in a stable way also within the useful region (Fig. 2), due to sector nonlinearity $[0,1]$, and it may be adapted for improving stability when $|e(t)| \ge \bar{\eta} e_{\max}$. FPI may start to operate from arbitrary initial detuning $e(0)$ within the FSR F_0, very likely outside the useful region where the expected PD signal is close to zero. Which asks for lock-in detection.

B. Lock-in detection and recovery (LDR)

LDR is achieved by an hybrid closed-loop strategy based on a stylized shape of the PD response, a doublet made as in Fig. 1 by four parts corresponding to the values of the automaton state $\underline{a}$ (encircled capital letters in Fig. 3):

1) unknown signal (DEFAULT),
2) zero or background signal (BACKGROUND),
3) signal inside extended region (SIGNAL),
4) zero crossing or linear region (LOCK-IN).

Control strategy has been designed to avoid false lock-in detection, which may occur due to parasitic zero-crossing, as well as to reduce lock-in detection time. The key strategy is a secure detection of the background signal, after which the extended region can be looked for. To this end, BACKGROUND state has been split into ZERO state, where background signal has to be confirmed, and SEARCH, where the extended region is looked for. Switching is driven either by time counter (doubly circled states in Fig. 3) as from ZERO to SEARCH and/or by thresholds on PD measure y_f. The output is the total commanded frequency $\underline{u}$ to actuators, whose rate may be modulated by automaton states. LOCK-IN triggers the linear controller. Escape from LOCK-IN is triggered by y_f and the model frequency detuning e (see below).

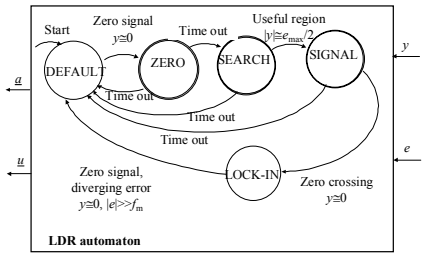

Fig. 3. Essential diagram of the LDR state automaton.

C. Embedded model

The embedded model (EM) is the design model to be embedded as the core of the linear regulator. It is written as a discrete-time (DT) dynamics starting from (4) and (7) and by decomposing e as in [5], into a single disturbance $d_e(i)$ and multiple command components $c_j(i)$, i being the generic discrete time and $j = 1,...,m$. The underlying time unit T is the command sampling step to be designed ($T = 0.1$ ms in [5] and [6]). It results

$$\begin{aligned} e(i) &= d_e(i) + c(i),\ c(i) = \sum_{j=1}^{m} c_j(i) \\ y_e(i) &= H_m(e(i)) + v(i) \end{aligned}, \qquad (9)$$

H_m being an approximation of the true H, to be estimated and coded as a look-up table, while v accounts for PD noise and aliasing errors due to sampling. Equation (9) must be completed with disturbance, actuator and sensor dynamics.

Disturbance dynamics models the disturbance class $\mathcal{D}$ which has to be rejected in order to guarantee target performance. As in [5], it is synthesized from the envelope of experimental/simulated PSD as the linear combination of white noise, random drifts and narrow-band noise tuned to specific frequencies. To guarantee robust observability, it can be shown the corresponding DT dynamics to be written as a series of elementary dynamics driven by 'arbitrary' DT signals $w_k(i)$ to be collected into a vector

$\mathbf{w}(i)$, as follows

$$d_e = w_0 + \mathbf{D}\cdot\mathbf{w}_d = \\ = w_0 + \mathbf{D}_1\cdot\left(w_1 + \mathbf{D}_2\cdot\left(w_2 + \cdots + \mathbf{D}_r\cdot w_r\right)\right) \quad ,(10)$$

where $\mathbf{w}^T = \left[w_0 \quad \mathbf{w}_d^T\right]$ and $\mathbf{D}\cdot\mathbf{w}_d$ denotes a linear DT operator acting on $\mathbf{w}_d(i)$ and its Z-transform with the notation $\mathbf{D}(z)\mathbf{w}(z)$. The elementary dynamics $\mathbf{D}_k$ may assume two forms

$$\mathbf{D}^{(1)}(z) = (z-1)^{-1},\ \mathbf{D}^{(2)}(z) = \\ = \alpha_k\left((z-1)^2 + \alpha_k(z-1) + \alpha_k\right)^{-1} \quad (11)$$

depending on drift or narrow-band assumption. F.i. the PSD in Fig. 4 (upper plot, from [6]) has been modelled as

$$d_e = w_0 + \mathbf{D}^{(1)}\cdot\left(w_1 + \mathbf{D}^{(1)}\cdot\left(w_2 + \mathbf{D}^{(3)}\cdot w_3\right)\right), \quad (12)$$

to include low-frequency drift and pendulum resonance.

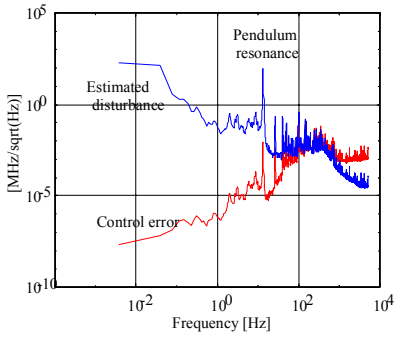

Fig. 4. PSD of the estimated disturbance, from [6].

Actuator dynamics $\mathbf{M}_j$ will be ordered as the low-frequency gains $b_j < \infty$, voltage-to-frequency: i.e. increasing gain b_j from $j=1$ to m correspond to decreasing bandwidth α_j. $\mathbf{M}_j$ Z-transform, assuming 1st order dynamics (2nd order may apply as in [11]), can be written as

$$c_j(z) = \mathbf{M}_j(z)u_j(z) = b_j\beta_j\left(z-1-\beta_j\right)^{-1}u_j(z), \quad (13)$$

less actuator noise and modelling errors. The fastest actuator, $b_1 = \min_j\{b_j\}$, is assumed to be dynamic-free, i.e. $\beta_1 = 1$ and the corresponding unit delay will be neglected.

PD dynamics can be usually neglected, but anti-aliasing filters have to be added to avoid spreading of wide-band disturbances (ground and acoustic noise) trough feedback. Experience [4] and formal proof suggests a decimated 1st order digital anti-aliasing filter to be adopted. Denote with $T_y = T/N$, $N \geq 1$ the PD sampling step and with k the corresponding discrete time. The anti-aliased PD measure $y(i)$ holds

$$y(i+1) = y(i) + \sum_{h=k}^{k+N-1} y_f(k)/N\,. \quad (14)$$

Among the advantages, the filter can be simply replicated into EM as a DT integrator, thus avoiding unmodelled dynamics while matching its bandwidth to digital control Nyquist frequency $f_{\max} = 0.5/T$. It means that the EM output y_m is related to PD output y_e, defined in (9), through the noise-free, BIBO unstable dynamics

$$y_m = \mathbf{M}\cdot y_e,\ \mathbf{M}(z) = (z-1)^{-1}. \quad (15)$$

By restricting to PD linear range, employing the approximation $H_m(e) = e$ and defining the total disturbance d including the sum v of PD noise and aliasing errors (the latter being very likely dominant) as $d = d_e + v$, the EM made by (9), (10), (13) and (15) can be written as

$$y_m = \mathbf{M}\cdot\left(b_1u_1 + \sum_{j=2}^{m}\mathbf{M}_j\cdot u_j + d\right),\ d = w_0 + \mathbf{D}\cdot\mathbf{w}_d\,. \quad (16)$$

D. *Command law (CL)*

As in [5], multiple commands will be exploited for apportioning disturbance rejection among different actuator capabilities. Denote with $\hat{d}$ an estimate of d provided by the Measurement Law (see below) and denote with $\hat{d}_j$ the portion to be tracked by actuator j subject to constraint $\hat{d}_m = \hat{d}$. Any actuator j will only track the low-frequency components of $\hat{d}_j$ defined by a low-pass filter, the *tracking dynamics*, to be designed and denoted by $\mathbf{V}_j$. As a consequence the following signal chain arises

$$\hat{d}_m = \hat{d} \\ \hat{d}_{j-1} = \left(\mathbf{I} - \mathbf{V}_j\right)\cdot\hat{d}_j,\ j = m,\ldots,2,\ \mathbf{S}_j = \mathbf{I} - \mathbf{V}_j \quad (17)$$

where $\mathbf{S}_j$ is the sensitivity proper to $\mathbf{V}_j$. To match actuator capabilities (gain and bandwidth), the sequence of sensitivities $\{\mathbf{S}_m,\ldots,\mathbf{S}_2\}$ will be designed to have increasing bandwidth as in [5]. This is done by appropriate tuning the eigenvalue set Λ_j of $\mathbf{V}_j$.

Tracking dynamics is designed as a dynamic input-output feedback $\mathbf{H}_j$ around the actuator model $\mathbf{M}_j$, where $\mathbf{H}_j$ must include a DT integrator to allow perfect tracking of dc components. F.i. in the 1st order case as in (13), the simplest feedback can be shown to hold

$$\mathbf{H}_j(z) = (z-1)^{-1}\left(h_{0j} + h_{1j}\left(z-1-\gamma_j\right)^{-1}\right). \quad (18)$$

It gives rise to a 3rd order low-pass filter $\mathbf{V}_j$ whose gains $\{\gamma_j, h_{0j}, h_{1j}\}$ are easily computed from the assigned Λ_j. Higher orders models $\mathbf{M}_j$, asking for more complex design of $\mathbf{H}_j$, will not be treated here.

The chain (17) has to be completed with the command apportionment equation

$$u_j = \underline{u}_j - \mathbf{H}_j\cdot\mathbf{S}_j\cdot\hat{d}_j = \underline{u}_j - \mathbf{H}_j\cdot\hat{d}_{j-1},\ j = m,\ldots,2\,, \quad (19)$$

the negative sign forcing disturbance rejection and $\underline{u}_j$ being the command computed by LDR (see Section B), if the case.

The fastest actuator (see [5]) must complete disturbance rejection with internal stability properties. To this end, it must force the effects of the bounded residual disturbance

$$\hat{e}_d = d - \hat{d} \tag{20}$$

to be bounded all over the feedback chain. This asks stabilizing the anti-aliasing filter (15) through state feedback so as to avoid $\hat{e}_d$ integration into drift. Owing to 1st order in (15), the scalar feedback $c_{CL} = -k\hat{y}$, in frequency units, from the model output estimate $\hat{y}$ (see Section E) is sufficient to the purpose, thus bringing to command law

$$u_1 = \underline{u}_1 - \left(k\hat{y} + \hat{d}_1\right)/b_1 . \tag{21}$$

The complete CL is made by (17), (19) and (21). CL mechanization in the DCU has to be completed by command digitization providing the digital command vector $\tilde{\mathbf{u}}(i)$ to plant DAC.

E. Measurement Law (ML)

Define the model error (or output innovation)

$$\hat{e}_y(i) = y(i) - \hat{y}(i) \tag{22}$$

as the discrepancy between the anti-aliased, decimated, PD measure y in (14) and the estimate $\hat{y}$ of the model output y_m in (16). The ML aims at estimating the driving noise $\mathbf{w}(i)$ of the class $\mathcal{D}$ under causality constraints. First, only a causal estimate $\overline{\mathbf{w}}(i)$ depending on $\hat{e}_y(i)$ and therefore correlated to past occurrences $\mathbf{w}(i-k)$, $k>0$ can be obtained, which, since Kalman filter, has been shown to be sufficient for updating $\hat{d}$ and guaranteeing the residual $\hat{e}_d$ in (20) to be (statistically) bounded. Second, $\hat{d}(i)$ must be estimated as a one-step prediction $\hat{d}(i) = \hat{d}(i/\overline{\mathbf{w}}(i-1))$ to allow CL mechanization one-step in advance, which implies $\hat{d}$ only to depend on the strictly causal part in (10):

$$\hat{d}(z) = \mathbf{D}(z)\overline{\mathbf{w}}_d(z) . \tag{23}$$

This entails ML to separate into a pair of feedback laws around EM (16) and driven by $\hat{e}_y$ as follows.

1) The dynamic feedback to predictable disturbance

$$\hat{d}(z) = \mathbf{D}(z)\overline{\mathbf{w}}_d(z) = \mathbf{D}(z)\mathbf{L}_d(z)\hat{e}_y(z) = \mathbf{H}_d(z)\hat{e}_y(z) \tag{24}$$

2) The dynamic feedback to unpredictable noise

$$\overline{w}_0(z) = \mathbf{H}_w\hat{e}_y(z) . \tag{25}$$

Then, model output $\hat{y}$, model error $\hat{e}_y$ and residual disturbance $\hat{e}_d$ can be expressed by

$$\begin{aligned} \hat{e}_y &= \mathbf{S}_w \cdot \left(y - \mathbf{M}\cdot u_{CL}\right) = \mathbf{S}_w \cdot \mathbf{M} \cdot \hat{e}_d \\ \hat{e}_d &= d - \hat{d} = \mathbf{S}_d \cdot d,\ \hat{y} = y - \hat{e}_y \end{aligned} , \tag{26}$$

upon definition of a pair of sensitivity operators

$$\begin{aligned} \mathbf{S}_w &= \left(I + \mathbf{H}_w \cdot \mathbf{M}\right)^{-1} \\ \mathbf{S}_d &= \left(I + \mathbf{H}_d \cdot \mathbf{S}_0 \cdot \mathbf{M}\right)^{-1} \end{aligned} , \tag{27}$$

which in turn combine into the overall ML sensitivity

$$\mathbf{S}_{ML} = \mathbf{S}_w \cdot \mathbf{S}_d = \left(I + \left(\mathbf{H}_w + \mathbf{H}_d\right)\cdot \mathbf{M}\right)^{-1} . \tag{28}$$

It can be shown from (17), (19) and (21) that the embedded model (16) can be mechanized in the DCU as

$$\hat{y} = \mathbf{M}\cdot\left(c_{CL} + \mathbf{H}_w \cdot \hat{e}_y\right) . \tag{29}$$

Then (29) and the feedback laws (24) and (25) constitute a state predictor driven by c_{CL} and $\hat{e}_y$. The gains of the feedback laws encoded in $\mathbf{H}_w$ and $\mathbf{L}_d$ are tuned by assigning the eigenvalue set Λ_{ML} of the predictor complementary sensitivity $\mathbf{V}_{ML} = I - \mathbf{S}_{ML}$. As the anti-aliased measure $y(i)$ is noise-free, eigenvalue tuning will be only constrained by unmodelled dynamics (see Sect. G) and not by measurement noise as in Kalman filter design.

F. Average performance

Let $\underline{e}(i)$ be the sampled average of the performance variable $e(t)$ over $T = NT_y$, T_y being the measurement sampling time as in Section C. From (9), (16) and the definition of d, it follows

$$\begin{aligned} \underline{e}(i) &= b_1 u_1(i) + \sum_{j=2}^{m}\left(\mathbf{M}_j \cdot u_j\right)(i) + \underline{d}(i) - \underline{v}(i) \\ \underline{e}(i) &= -k\hat{y}(i) + \underline{\hat{e}}_d(i) - \underline{v}(i) \end{aligned} , \tag{30}$$

where $\underline{\hat{e}}_d(i) = \underline{d}(i) - \hat{d}(i)$. Then by introducing the command law feedback operator

$$\mathbf{V}_{CL} = \left(I + k\mathbf{M}\right)^{-1} k\mathbf{M} = k(z-1-k)^{-1} \tag{31}$$

one obtains

$$\underline{e} = -\underline{v} + \left(I - \mathbf{V}_{CL}\cdot\mathbf{M}^{-1}\cdot\left(I - \mathbf{S}_w\right)\cdot\mathbf{M}\right)\cdot\mathbf{S}_d\cdot\underline{d} \tag{32}$$

which in SISO case and assuming $\mathbf{V}_{CL} \simeq I$ simplifies to

$$\underline{e} \simeq -\underline{v} + \mathbf{S}_{ML}\cdot\underline{d} . \tag{33}$$

Finally, by reusing definition $d = d_e + v$, one obtains the classical equation

$$\underline{e} \simeq -\mathbf{V}_{SM}\cdot\underline{v} + \mathbf{S}_{SM}\cdot\underline{d}_e , \tag{34}$$

where $\underline{v}(i)$ and $\underline{d}_e(i)$ are practically aliasing-free, being the time average of $v(t)$ and $d_e(t)$. Equation (34) shows performance to be limited by low-frequency components of $\underline{v}$, which may be affected by non-stationary components like flicker (PD electronics), and by the bandwidth of $\mathbf{V}_{ML}$.

G. Robust stability versus unmodelled dynamics

Performance and stability are affected by unmodelled dynamics, not explicitly formulated for sake of brevity. F.i. residual disturbance $\hat{e}_d$ may be affected by an oversimplified dynamics $\mathbf{M}_j$ in the frequency region close

to control rate $f_c = 1/T$. In which case, internal stability is no more guaranteed by (21), as $\hat{e}_d$, now command dependent, creates a new closed-loop which is out-of-design and, worse, uncertain. Stability and performance are recovered as in [5], by constraining the eigenvalues of the tracking dynamics $\mathbf{V}_j$ and of the predictor sensitivity $\mathbf{S}_{ML}$ to free $\hat{e}_d$ from the unmodelled dynamics effects below a certain threshold. This is first obtained through analytic approximations of the unmodelled dynamics and then refined through simulated experiments and field tests. Of course, eigenvalue constraints will restrict the bandwidth of $\mathbf{V}_j$ and $\mathbf{V}_{ML}$, thus degrading disturbance rejection.

IV. EXPERIMENTAL AND SIMULATED RESULTS

Experimental results refer to

1) a ground test-bed to demonstrate FPI in the sub-nanometric dimensional stabilization (in vacuum) of space optics with mass >1 kg and size ≥ 1 m [3], [4],
2) digital frequency stabilization of a monolithic laser source through a set of coordinated actuators (acousto-optic modulator, PZT ceramics, thermal control) [5],
3) an instrument for space micro-thruster qualification, where the laser source frequency is actuated by PZT ceramics and thermal control to track and measure the length detuning of a Fabry-Pérot cavity due to micro-thruster force [6].

Simulated results refer to the ground breadboard of a metrology line, now under construction, for measuring and possibly stabilizing thermo-elastic deformations of the GAIA telescope [4]. Metrology lines are a development from the test-bed mentioned in [3]. A stabilized laser frequency is detuned by an acousto-optic modulator to track and measure the length detuning of a cavity mounted on the optics.

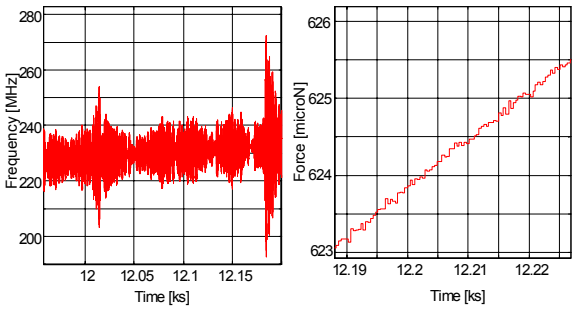

Fig. 5. Left: raw frequency measures. Right: filtered force measures.

Fig. 4 shows the PSD of the estimated length detuning (upper plot) of the cavity under zero force, corresponding to the sum of instrument and laser source noise. The lower plot is the control jitter PSD showing tracking of length detuning up to 100 Hz, so as to include the parasitic pendulum resonance at 13 Hz for calibration. Actually the parasitic resonance, due instrument imbalance and ground noise, affects the length measurements but it can be filtered for revealing length measures up to 2 Hz with a resolution better than 1 μN, as Fig. 5 shows (see also [6]).

Experimental results showing command apportionment can be found in [5] and [11]. Fig. 6 shows command apportionment for the suspended cavity of the micro-thruster instrument where a voice coil has been added to laser PZT and thermal control to suppress parasitic resonance. As pointed out in [5], although a single command rate, $f_c = 10$ kHz, is adopted for all commands to simplify mechanization, multi-rate actuation naturally results due to progressive bandwidth restriction and resolution relaxation from faster to slower actuators.

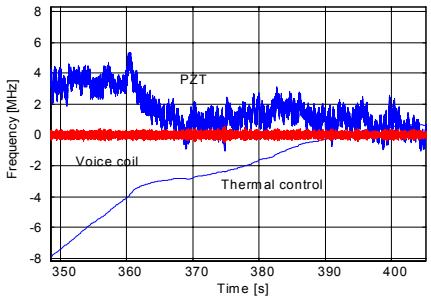

Fig. 6. Command apportionment from [11].

REFERENCES

[1] A.E. Siegman, *Lasers,* Sausalito (CA): Univ. Science Books, 1986.

[2] R. W. Drever, J.L. Hall, F.W. Kowalski, J. Hough, G.M. Ford, A.J. Munley *et al.*, "Laser phase and frequency stabilization using an optical resonator", *Appl. Phys. B*, 1983, 21, 97-105.

[3] F. Bertinetto and E. Canuto, "Sub-nanometer digital positioning of large bodies by Fabry-Pérot interferometry", *Opt. Eng.,* 40 (1), 2001, 76-80.

[4] E. Canuto "Sub-nanometric optics stabilization in view of the GAIA astrometric mission", *Control Eng. Practice,* 11 (5), 2003, 569-578.

[5] E. Canuto and A. Rolino "Multi-input digital frequency stabilization of monolithic lasers", *Automatica*, 40(12), 2004, 2139-2147.

[6] E. Canuto and A. Rolino "An automated interferometric balance for micro-thrust measurement", *ISA Trans.*, 43(2), 2004, 169-187.

[7] S.A. Webster, M. Oxborrow and P. Gill, "Subhertz-linewidth Nd:YAG laser", *Opt. Lett.,* 29, 1497, 2004.

[8] E. Canuto and Musso F., "Dynamics of Fabry-Pérot cavities", Tech. Rep. No.1, 2005, Politecnico di Torino, Space Precision Automatics.

[9] B. Caron, A. Dominjon, F. Marion, L. Massonnet, D. Morand, B. Mours *et al.* "Status of the VIRGO experiment". *Nucl. Instrum. Meth.* 360, 1995, 258-262.

[10] A. Abramovici, Althouse, J. Camp, D. Durance, J. A. Giaime, A. Gillespie *et al.* "Improved sensitivity in a gravitational wave interferometer and implications for LIGO". *Physics Letters A* 218(8), 1996, 157-163.

[11] E. Canuto and A. Rolino, "Active vibration suppression in a suspended Fabry-Pérot cavity", in *Proc. 2004 American Control Conf.,* Boston (MA, USA), June 30-July 2, 3660-3665.

[12] E. Canuto, F. Musso and D. Andreis "Embedded Model Control: application to electrohydraulics", submitted to *2005 IEEE Med. Control Conf.,* Cyprus.

[13] E. Canuto Controlli Automatici, Parte II. Controllo digitale. Turin (Italy), CELID, 2002 (in Italian).